GSA DATA REPOSITORY 2015173

Geological setting

The Kazusa Group is one of the thickest (approximately 3000 m) and best exposed Lower and Middle Pleistocene sedimentary successions in the Japanese islands (e.g., Ito, 1998; Kazaoka et al., accepted). Well-preserved microfossils (e.g., Oda, 1977; Sato et al., 1988; Cherepanova et al., 2002) and oxygen isotope stratigraphy (Okada and Niitsuma, 1989; Pickering et al., 1999; Tsuji et al., 2005) place the Kazusa Group at between 2.4 and 0.5 Ma. The Matuyama–Brunhes boundary (MBB) and Byk-E tephra occur in the Kokumoto Formation, Kazusa Group. The Kokumoto Formation represents an expanded and well-exposed sedimentary succession across the Lower–Middle Pleistocene boundary, especially at the Chiba composite section, which comprises the Tabuchi (35˚17.66'N; 140˚8.79'E), Yanagawa (35˚17.15'N; 140˚7.88'E), and Kogusabata (35˚18.52'N; 140˚11.89'E) sections (Figure 1B and S. Figure 1). These routes are adjacent and contiguous throughout the Lower–Middle Pleistocene boundary interval. Marine oxygen isotope records by Pickering et al. (1999) and Okada and Niitsuma (1989) reveal a continuous record from MIS 21 to MIS 18, with glacial–interglacial cycles corresponding to sandstone- and siltstone-dominated units, respectively. This lithological variation generally corresponds to higher and lower sedimentation rate, respectively (S. Table 1). The Byk-E tephra is widely distributed in the area, and provides an excellent stratigraphic marker between the Tabuchi, Yanagawa, and Kogusabata sections (S. Figures 1 and 2). Takeshita et al. (2005) reported that the Byk-E tephra is correlated with the YUT4 or 5 tephra beds from the Older Ontake Volcano, central Japan. This tephra bed is therefore

considered an excellent stratigraphic marker for the Lower–Middle Pleistocene boundary in the Kokumoto Formation of the Kazusa Group. In this study, paleomagnetic samples were collected from the Tabuchi section (along the Yoro River) and Yanagawa section (Yana River), and oxygen isotope samples are from the Yanagawa and Kogusabata (Kogusabata River) sections (S. Figure 2).

Paleomagnetic and rock magnetic experiments and results

Rock and paleomagnetic samples were taken using a portable drill and were oriented using a magnetic compass. Turbidite sandstones were avoided. In order to determine the grain size and composition of magnetic minerals, and their stability for thermal demagnetization (ThD) analysis, the rock magnetic measurements outlined below were carried out. Remanence measurements were made using a (2-G Enterprises) three-axis cryogenic magnetometer installed in a magnetically shielded room.

Magnetic hysteresis was measured for selected samples using an alternating gradient magnetometer (Princeton Measurements Corporation MicroMag 2900) (S. Figure 3A). The ratio of the saturation magnetization to saturation remanence (M_{rs}/M_s) is commonly used as a proxy for the magnetic grain size of ferrimagnetic particles (Day et al., 1977). In general, higher and lower values of M_{rs}/M_s correspond to finer and coarser magnetic grain size, respectively. Most samples fall within a limited range of magnetic grain sizes that correspond to pseudo-single-domain (PSD) sizes (S. Figure 3B).

Thermomagnetic experiments were performed on eight sets of selected samples using a thermomagnetic balance (NMB-89; Natsuhara Giken) at the Center for Advanced Marine

Core Research, Kochi University. The samples were heated in air or under vacuum from 100 to 700 °C in a field of 300 mT (S. Figure 4A and B). Samples heated in air have a single Curie temperature at 580 °C with a pronounced increase between 400 and 450 °C, which indicates the creation of a ferrimagnetic mineral phase. On cooling below the Curie temperature, however, the thermomagnetic curves have a lower magnetization compared to the respective heating curves. This indicates that the ferrimagnetic mineral created between 400 and 450 °C was further altered during heating to form a material with higher Curie/Neal temperature, such as hematite. On the other hand, the samples heated in a vacuum undergo an increase in magnetization during cooling, with a single Curie temperature at 580 °C. This suggests that substantial alteration occurred, but only above the Curie temperature.

Progressive thermal demagnetization (ThD) of composite 3-axis IRMs (Lowrie, 1990) for eight sets of selected samples was conducted to identify the coercivity, intensity of acquired IRM, and blocking temperature of magnetic minerals in the sediments. Three-axis IRM components were acquired in direct magnetic fields of 0.03 (soft), 0.5 (medium), and 1.5 T (hard), and subsequent progressive ThD was conducted from 100 °C to 700 °C at 20–50 °C intervals in air or under vacuum (S. Figure 5A and B). The samples heated in air undergo a major decrease in intensity for the 0.03 and 0.5 T components between 450 °C and 580 °C, which indicates the existence of a magnetic mineral with soft to medium coercivity, probably magnetite or low-Ti titanomagnetite. Subsequently, small IRM decreases were observed above 600 °C for all components. This indicates that samples heated in air contain a small contribution of a higher temperature component, such

as hematite. In contrast, magnetizations of samples heated under vacuum are mostly carried by the 0.03 and the 0.5 T components, and demagnetized below 580 ˚C, which indicates a dominance of magnetite.

Typical stepwise alternating field and thermal demagnetization (AFD, ThD) results are shown in Zijderveld diagrams (Zijderveld, 1967) in S. Figure 6 (A–D). Stepwise ThD (up to 680 °C, with 10–50 °C temperature increments) revealed that most samples have a characteristic component that decays toward the origin of the plot at 300–580 °C. This unblocking temperature indicates that the main magnetization carrier in these samples is magnetite (titanomagnetite), which is consistent with the thermomagnetic results discussed above. Characteristic remanent magnetization (ChRM) directions, calculated by principal component analysis (Kinschvink, 1980), for normal and reversed polarity sites are antipodal (Figure 1, S. Figure 2, and S. Table 1), which indicates that the Kokumoto Formation preserves reliable primary magnetizations at the Chiba composite section.

Oxygen isotope analysis

Rock samples for oxygen isotope stratigraphy were collected from the Yanagawa and Kogusabata sections of the Chiba composite section at 76 horizons (68 of them were used for the analysis) covering a 100.2-m succession (S. Figure 2). Samples were disaggregated using $NaSO_4$, and the non-magnetic fraction including foraminifera was concentrated using an isodynamic separator. We manually picked benthic foraminifera from the non-magnetic fraction for each sample. Oxygen isotopic measurements were performed with an Isoprene mass spectrometer installed in the Kochi Core Center (KCC) using CO-1 and NBS-19 as

standard samples to calibrate the measured isotopic values to the Vienna Pee Dee Belemnite (VPDB). The standard deviation of the oxygen isotopic measurements was calculated as 0.09 ‰ from 31 measurements of CO-1 working standard specimens. We used *Bolivinita quadrilatera* and *Cibicidoides* spp., which were yielded dominantly from this succession, for isotopic measurements. Okada et al. (2012) reported that *Bolivinita quadrilatera* has $\delta^{18}O$ values identical with the genus *Uvigerina*, which is though to have an equilibrium $\delta^{18}O$ value with the bottom water. We therefore corrected the $\delta^{18}O$ values of *Cibicidoides* spp. to those of *Bolivinita quadrilatera* by adding 0.64 ‰, which is the average $\delta^{18}O$ difference between *Cibicidoides* and *Uvigerina* (Shackleton and Hall, 1984).

U–Pb zircon dating

Zircon grains from the Byk-E tephra were concentrated using conventional mineral-separation techniques, including pulverizing the sediment, heavy liquid separation with methylene iodide, and magnetic separation using an isodynamic magnetic separator. Adequate amounts of zircons (> 200 grains) were randomly handpicked from each sample. The external morphologies of collected grains were observed using a low vacuum scanning electron microscope (LV-SEM; JEOL JSM-5900LV) at the National Institute of Polar Research, Japan. The zircon grains were mounted together with reference zircons in an epoxy resin disc. After curing, these discs were polished to obtain cross-sections through the grains. In order to investigate the internal structures of individual zircons, backscattered electron (BSE) and cathodoluminescence (CL) images were obtained using a SEM (JEOL JSM-5900LV). These images guided the selection of analytical spots.

U-Pb analyses were performed using a SHRIMP-II (sensitive high-resolution ion microprobe) at the National Institute of Polar Research, Japan. The surfaces of grain mounts were washed in 2% HCl and ultrapure water to remove any lead contamination, and were then coated with gold prior to analysis. An O_2^- primary ion beam of ~11 nA was used to sputter an analytical spot 40 μm in diameter on the polished mount. The procedures for Pb and U isotopic analyses of zircon follow Horie et al. (2013). In this study, TEMORA2 ($^{206}Pb/^{238}U$ age: 416.78 ± 0.33 Ma; Black et al., 2004) and SL13 (U concentration: 238 ppm; Claoué-Long et al., 1995) were used as reference materials for the U-Pb analysis. The U-Pb data were reduced in a manner similar to that described by Williams (1998), by using the SQUID2 Excel macro of Ludwig (2009). Correction for common Pb was made on the basis of measured ^{204}Pb and the model for common Pb compositions proposed by Stacey and Kramers (1975). Weighted mean ages at the 95% confidence level and apparent ages were calculated from $^{206}Pb/^{238}U$ ratios corrected by ^{207}Pb assuming $^{206}Pb/^{238}U$–$^{207}Pb/^{235}U$ age-concordance. The pooled ages presented in this study are all after correction for common Pb and were calculated using the Isoplot/Ex software (Ludwig, 2012).

For zircons younger than ~1 Ma, a deficit of ^{206}Pb due to initial Th/U disequilibrium caused by exclusion of ^{230}Th should not be disregarded (e.g., Schärer, 1984). Initial ^{238}U–^{230}Th disequilibrium was corrected using the method described by Parrish and Noble (2003) and references therein. Correction of $^{206}Pb/^{238}U$ dates for the deficit requires estimation of the Th/U of zircon ($Th/U_{[zircon]}$) and that of the magma from which the zircon crystallized ($Th/U_{[magma]}$). In this study, the $Th/U_{[magma]}$ ratio was assumed to be 5.82 ± 0.03

(RSD: 0.5%), as estimated using volcanic glass from the Byk-E tephra analyzed by ICP-MS.

Hand-picked glass shards were ultrasonicated in 1% HCl for 1 h, in de-ionized water (18 MΩ) for 3 h, and dried. The shards were pulverized with an agate mortar and pestle, and digested in concentrated HF and $HClO_4$. The dried sample was transferred to nitrate with 6M-HNO_3, and diluted with 2 % HNO_3 for analyses. Concentrations of Th and U were analyzed by ICP-MS (Agilent 7500ce) at JAMSTEC using the analytical protocol described by Chang et al. (2003). Th and U were analyzed five times to improve precision using 10 s data acquisition on each mass peak in one run. Analytical precisions were 0.4 %RSD (% relative standard deviation (1 sigma)) on both Th (8.44 ± 0.04 ppm) and U (1.45 ± 0.01 ppm) for the Byk-E Tephra. The same analysis on a BCR-2 rock standard (United States Geological Survey) yielded 0.7 (5.94 ± 0.04 ppm Th) and 0.6 %RSD (1.71 ± 0.01 ppm U), respectively, with external reproducibility of the averaged value of -0.2 %RD (% relative deviation) for Th and 0.9 %RD for U from the GeoReM preferred values of 5.95 ppm (Th compiled value of two analyses) and 1.69 ppm (U compiled value), respectively (Jochum et al., 2007).

REFRENCES CITED

Black, L.P., Kamo, S.L., Allen, C.M., Davis, D.W., Aleinikoff, J.N., Valley, J.W., Mundil, R., Campbell, I.H., Korsch, R.J., Williams, I.S., and Foudoulis, C., 2004, Improved $^{206}Pb/^{238}U$ microprobe geochronology by the monitoring of a trace-element-related matrix effect; SHRIMP, ID-TIMS, ELA-ICP-MS and oxygen isotope documentation

for a series of zircon standards: Chemical Geology, v. 205, p. 115–140.

Chang, Q., Shibata, T., Shinotsuka, K., Yoshikawa, M., and Tatsumi, Y., 2003, Precise determination of trace elements in geological standard rocks using inductively coupled plasma mass spectrometry: Frontier Research on Earth Evolution, v. 1, p. 575–362.

Cherepanova, M.V., Pushkar, V.S., Razjigaeva, N., Kumai, H., and Koizumi, I., 2002, Diatom biostratigraphy of the Kazusa Group, Boso Peninsula, Honshu, Japan: The Quaternary Research (Daiyonki Kenkyu), v. 41, p. 1–10.

Claoué-Long, J.C., Compston, W., Roberts, J., and Fanning, C.M., 1995, Two Carboniferous ages: a comparison of SHRIMP zircon dating with conventional zircon ages and $^{40}Ar/^{39}Ar$ analysis, *in* Berggren, W.A., Kent, D.V., Aubrey, M.P., and Hardenbol, J. eds., Geochronology Time Scales and Global Stratigraphic Correlation: Tulsa, Society for Sedimentary Geology Special Publication, v. 54, p. 3–21.

Day, R., Fuller, M., and Schmidt, V.A., 1977, Hysteresis properties of titanomagnetites: Grain-size and compositional dependence: Physics of the Earth and Planetary Interiors, v. 13, p. 260–267.

Dunlop, D.J., 2002, Theory and application of the Day plot (M_{rs}/M_s versus H_{cr}/H_c) 1. Theoretical curves and tests using titanomagnetite data: Journal of Geophysical Research, v. 107, doi:10.1029/2001jb000486.

Horie, K., Takehara, M., Suda, Y., and Hidaka, H., 2013, Potential Mesozoic reference zircon from Unazuki plutonic complex: geochronological and geochemical characterization: Island Arc, v. 22, p. 292–305.

Ito, M., 1998, Submarine fan sequences of the lower Kazusa Group, a Plio-Pleistocene

forearc basin fill in the Boso Peninsula, Japan: Sedimentary Geology, v. 122, p. 69–93.

Jochum, K.P., Nohl, U, Herwig, K., Lammel, E., Stoll, B., and Hofmann, A.W., 2007, GeoReM: a new geochemical database for reference materials and isotopic standards: Geostandards and Geoanalytical Research, v. 29, p. 333–338, DOI: 10.1111/j.1751-908X.2005.tb00904.x.

Kazaoka, O., Suganuma, Y., Okada, M., Kameo, K., Head, M.J., Yoshida, T., Sugaya, N., Kameyama, S., Ogitsu, I., Nirei, H., Aida, N., and Kumai, H., Stratigraphy of the Kazusa Group, Boso Peninsula: an expanded and highly-resolved marine sedimentary record from the Lower and Middle Pleistocene of Central Japan: Quaternary International (accepted).

Kirschvink, J.L., 1980, The least-squares line and plane and the analysis of palaeomagnetic data: Geophysical Journal of the Royal Astronomical Society, v. 62, p. 699–718.

Lowrie, W., 1990, Identification of ferromagnetic minerals in a rock by coercivity and unblocking temperature properties: Geophysical Research Letters, v. 17, p. 159–162.

Ludwig, K.R., 2009, SQUID 2: a user's manual: Berkeley, Berkeley Geochronology Center Special Publication 2, 104 P.

Ludwig, K.R., 2012, Isoplot 3.75–4.15: a geochronological toolkit for Microsoft Excel: Berkeley, Berkeley Geochronology Center Special Publication 5, 75 p.

Mitsunashi, T., Yazaki, K., Kageyama, K., Shimada, T., Ono, E., Yasukuni, N., Makino, T., Shinada, Y., Fujiwara, K., and Kamata, S., 1961, Geological maps of the oil and gas field of Japan no. 4, Futtsu-Otaki: Geological Survey of Japan, scale 1:50,000, 1 sheet.

Oda, M., 1977, Planktonic foraminiferal biostratigraphy of the late Cenozoic sedimentary sequence, Central Honshu, Japan: Science Reports of the Tohoku University, Second Series, Geology, v. 48, p. 1–76.

Okada, M., and Niitsuma, N., 1989, Detailed paleomagnetic records during the Brunhes–Matuyama geomagnetic reversal and a direct determination of depth lag for magnetization in marine sediments: Physics of the Earth and Planetary Interiors, v. 56, p. 133–150.

Okada, M., Tokoro, Y., Uchida, T., Arai, Y., and Saito, K., 2012, An integrated stratigraphy around the Plio-Pleistocene boundary interval in the Chikura Group, southernmost part of the Boso Peninsula, central Japan, based on data from paleomagnetic and oxygen isotopic analyses: Journal of Geological Society of Japan, v. 118, p. 97–108 (in Japanese with English abstract).

Parrish, R.R., and Noble, N.R., 2003, Zircon U-Th-Pb geochronology by isotope dilution-thermal ionization mass spectrometry (ID-TIMS), *in* Hanchar, J.M. and Hoskin, P.W.O., eds., Zircon: Reviews in Mineralogy and Geochemistry, 53, Washington D.C., Mineralogical Society of America, p. 182–213.

Pickering, K.T., Souter, C., Oba, T., Taira, A., Schaaf, M., and Platzman, E., 1999, Glacio-eustatic control on deep-marine clastic forearc sedimentation, Pliocene–mid-Pleistocene (c. 1180–600 ka) Kazusa Group, SE Japan: Journal of the Geological Society, v. 156, p. 125–136.

Sato, T., Takayama, T., Kato, M., Kudo, T., and Kameo, K., 1988, Calcareous microfossil biostratigraphy of the uppermost Cenozoic formations distributed in the coast of the

Japan Sea, Part 4: Conclusion: Journal of the Japanese Association of Petroleum Technologist, v. 53, p. 474–491 (in Japanese with English abstract).

Shackleton, N.J., and Hall, M.A., 1984, Oxygen and carbon isotope stratigraphy of DSDP Hole 552A: Plio-Pleistocene glacial history: Initial Reports of the Deep Sea Drilling Project, v. 81, p. 599–609.

Schärer, U., 1984, The effect of initial ^{230}Th disequilibrium on young U–Pb ages: the Makalu case, Himalaya: Earth and Planetary Science Letters, v. 67, p. 191–204.

Stacey, J.S., and Kramers, J.D., 1975, Approximation of terrestrial lead isotope evolution by a two-stage model: Earth and Planetary Science Letters, v. 26, p. 207–221.

Takeshita, T., Miyake, Y., and Sakai, J., 2005, Correlation of the tephra beds in the Middle Pleistocene Older Ontake Volcano with those in the Kazusa Group in Boso Peninsula, central Japan: Journal of Geological Society of Japan v. 111, p. 417–433 (in Japanese with English abstract).

Tsuji, T., Miyata, Y., Okada, M., Mita, I., Nakagawa, H., Sato, Y., and Nakamizu, M., 2005, High-resolution chronology of the lower Pleistocene Otadai and Umegase Formations of the Kazusa Group, Boso Peninsula, central Japan: chronostratigraphy of the JNOC TR-3 cores based on oxygen isotope, magnetostratigraphy and calcareous nannofossil: Journal of Geological Society of Japan v. 111, p. 1–20 (in Japanese with English abstract).

Williams, I.S., 1998, U–Th–Pb geochronology by ion microprobe. In: McKibben, M.A., Shanks III, W.C. and Ridley, W.I., eds., Applications of Microanalytical Techniques to Understanding Mineralizing Processes: Reviews in Economic Geology, vol. 7, p. 1–35.

Zijderveld, J.D.A., 1967. A.C. demagnetization of rocks: analysis of result. *in* Collinson, D.W., Creer, K.M. and Runcorn, S.K., eds., Methods in Paleomagnetism: New York, Elsevier, p. 254–286.

SUPPLEMENTAL TABLES AND FIGURE CAPTIONS

Supplemental Table 1. Inclinations and declinations of characteristic remanent magnetizations (ChRMs), VGP latitudes and longitudes calculated from the ChRMs, and the stratigraphic distance from the Byk-E tephra used for Figure 1. Each ChRM is derived from more than 5 vector end-points between 300 and 500 °C for a progressive thermal demagnetization result. Sample locality information is shown below the paleomagnetic data.

Supplemental Table 2. Averaged oxygen isotopic ratios of benthic foraminiferal tests, sample localities, stratigraphic horizons, and the age model used for Figure 1. Sedimentation rates are calculated from stratigraphic intervals between sample horizons without sandstone layers.

Supplemental Table 3. U-Th data and U-Pb ages of zircon grains used for Figure 2A and 2B. Table 3A contains data for the 24 youngest zircon grains, used to calculate the age of the Byk-E tephra. The zircon grains with older U-Pb ages are compiled in Table 3B.

Supplemental Figure 1. Geologic map of the Kazusa Group with marker tephra beds and

lithofacies indicated around the Yoro and Yana rivers, modified from Mitsunashi et al. (1961).

Supplemental Figure 2. Detailed stratigraphic correlations between the Yanagawa, Tabuchi, and Kogusabata sections (A), and magneto- and oxygen isotope stratigraphy (B). The stratigraphic correlations are based on lithological changes and the marker tephra beds Ku1, Ku2, Tas, Tap, Byk-A, and Byk-E (Kazaoka et al., accepted). Samples YNG01–53 from the Yanagawa section and TBH01–71 from the Tabuchi section were used for the paleomagnetic measurements. The remaining samples, from the Yanagawa section (YG01–06, YN01–20, YW01–11) and the Kogusabata section (KG01–39) were used for oxygen isotope analyses. The oxygen isotopic data from the Yanagawa and Kogusabata sections are adjusted to the Yoro River stratigraphic scale.

Supplemental Figure 3. Hysteresis loops for representative samples (a). Red and blue are uncorrected then corrected for paramagnetic slopes, respectively. Day plot of hysteresis parameters for selected samples (b). Abbreviations are: SD: single-domain, PSD: pseudo-single-domain, MD: multi-domain; after Dunlop (2002).

Supplemental Figure 4. Examples of thermomagnetic analysis for selected samples from 100 to 700°C. Arrows represent heating and cooling.

Supplemental Figure 5. Progressive thermal demagnetization of the three-component IRMs

(0.03, 0.5, 1.5 T).

Supplemental Figure 6. Examples of stepwise alternating field (AF) and thermal (Th) demagnetization (a–f). The filled and open circles correspond to projections onto the horizontal and vertical planes, respectively.

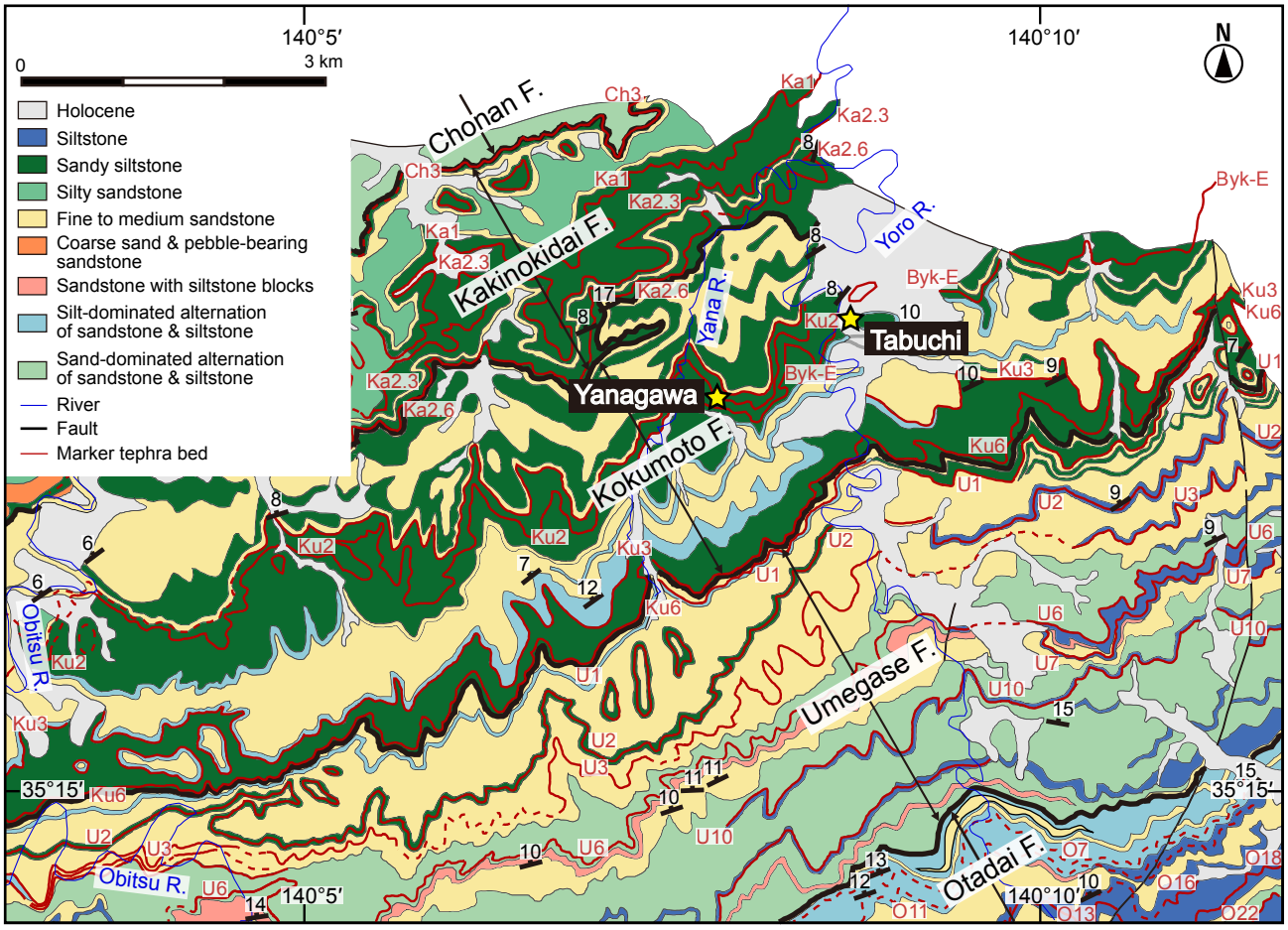

Suganuma et al. S. Figure 1

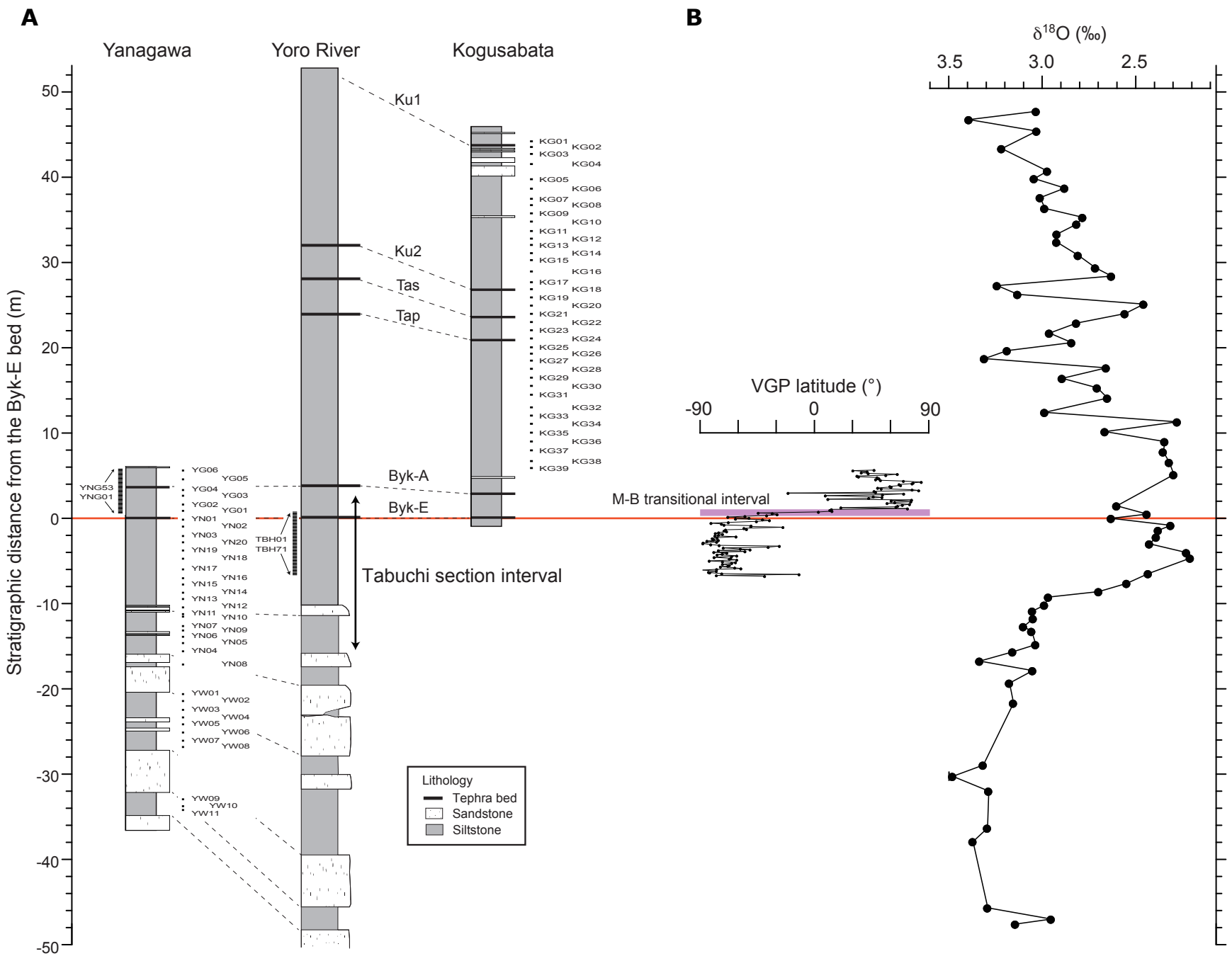

Suganuma et al., S. Figure 2

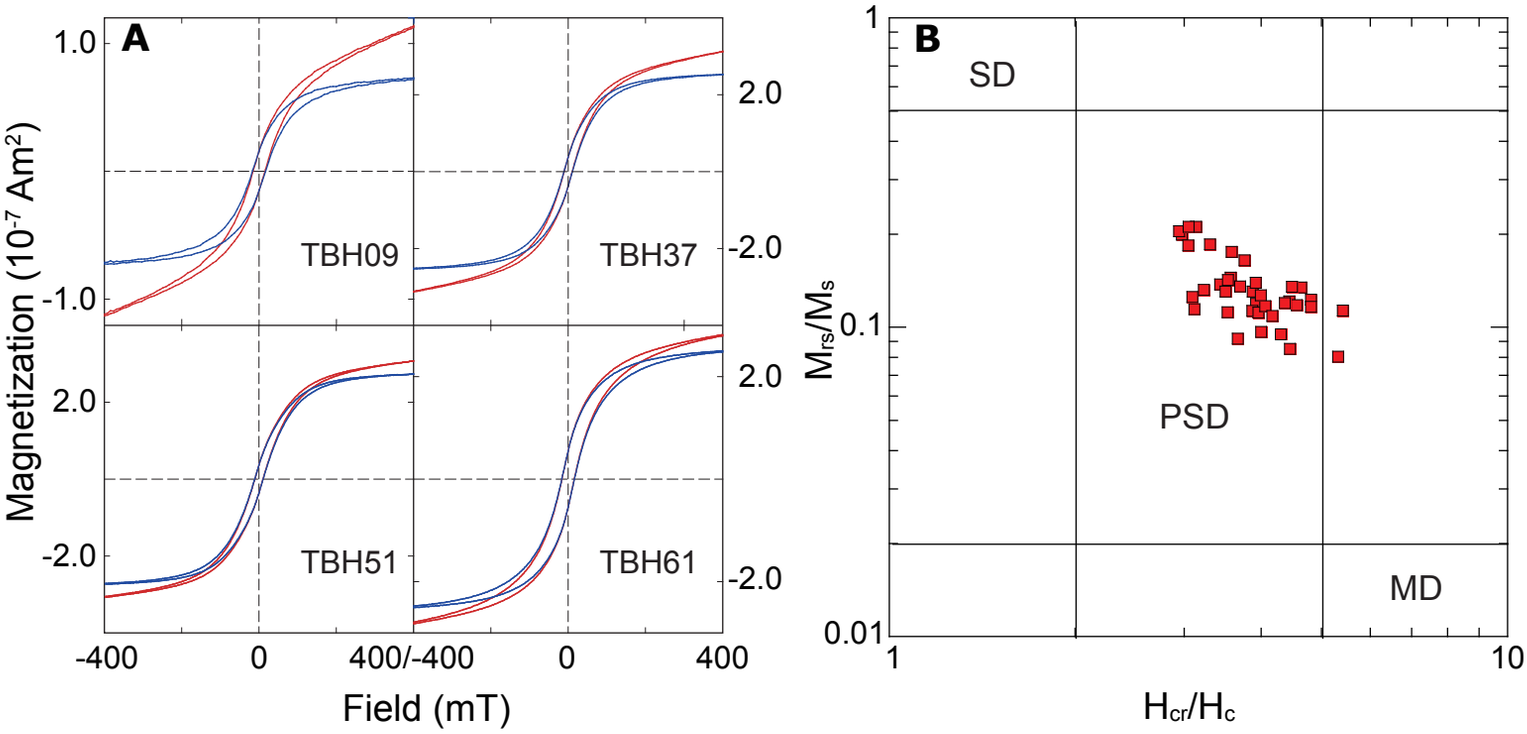

Suganuma et al., S. Figure 3

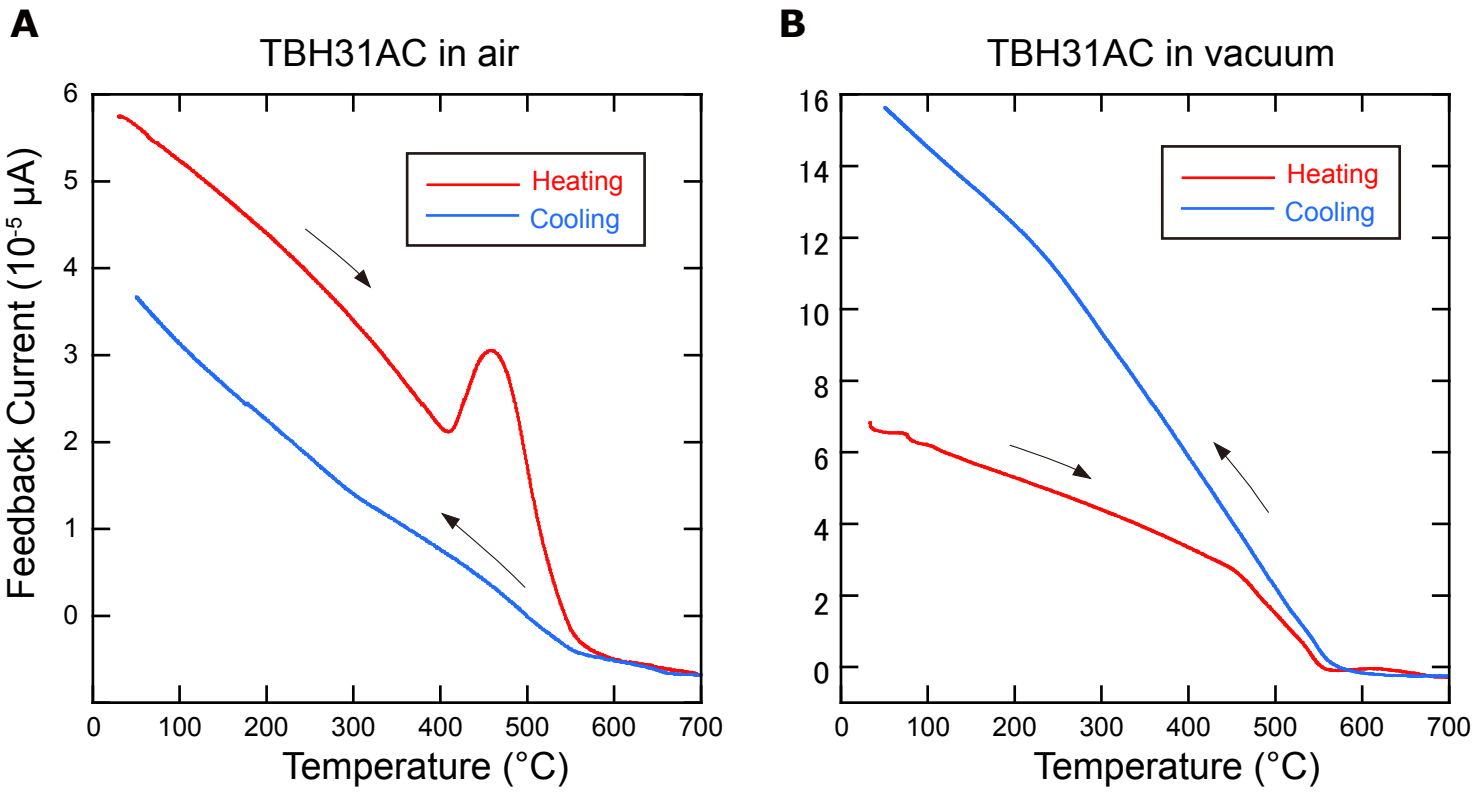

Suganuma et al., S. Figure 4

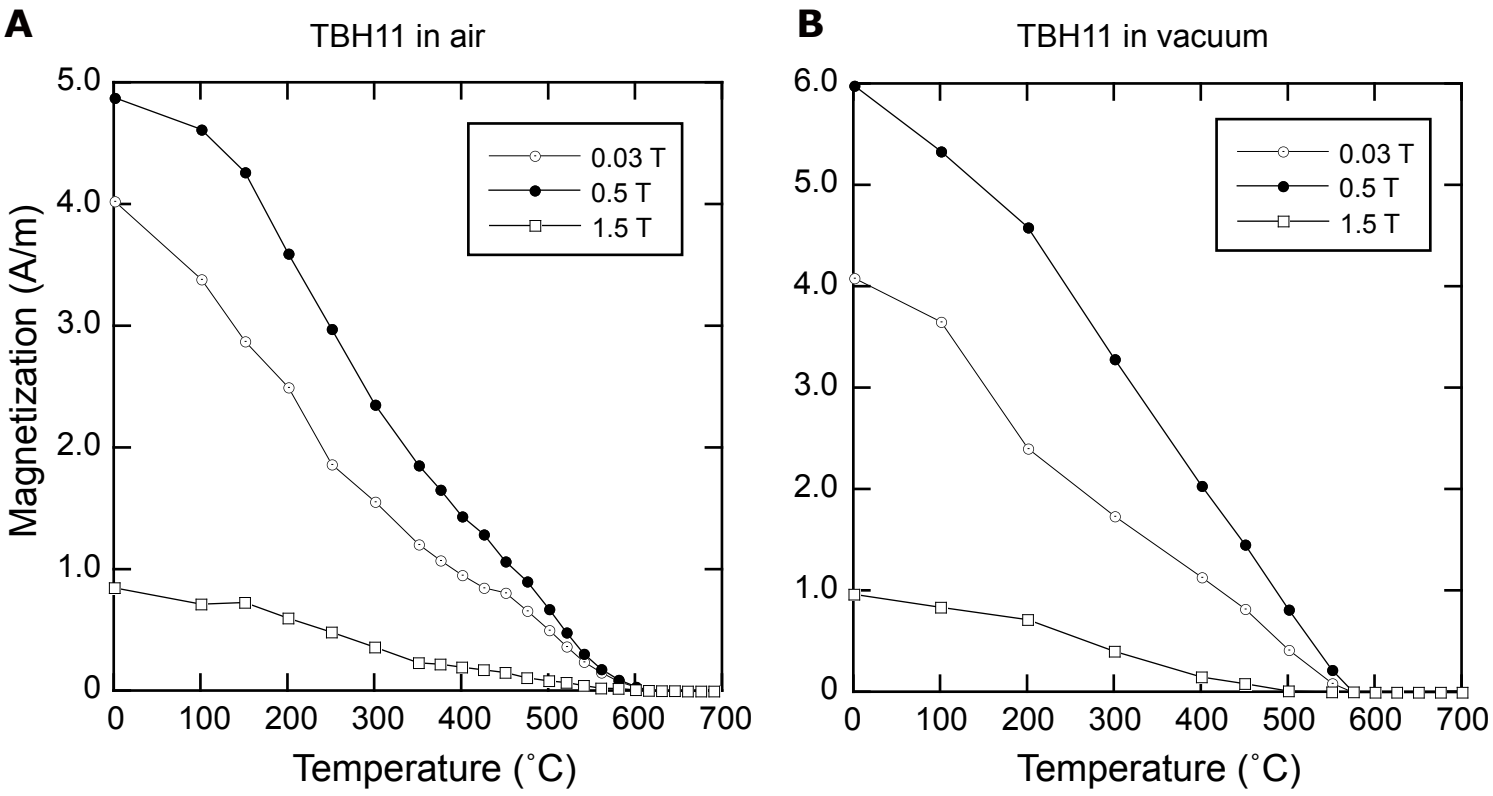

Suganuma et al., S. Figure 5

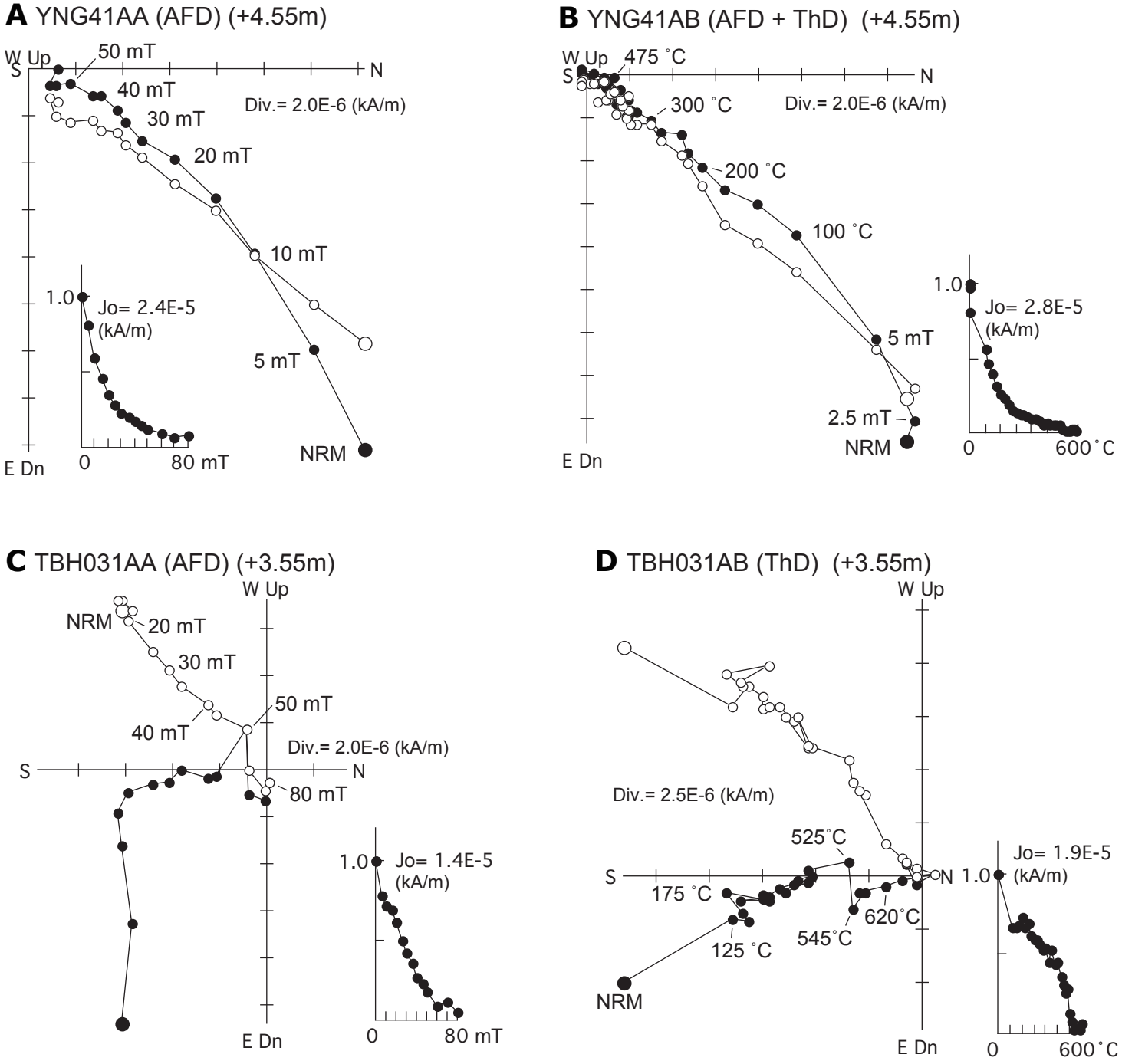

Suganuma et al., S. Figure 6

S.Table 1

Sample name	Stratigraphic distance from the Byk-E bed (m)	Age derived by $d^{18}O$ correlation (ka)	ChRM Declination (˚)	ChRM Inclination (˚)	MAD (˚)	VGP latitude (˚)	VGP longitude (˚)	Comments
YNG53AB	5.75	765.57	48.5	44.9	5	47.9	-132.1	
YNG52AB	5.65	765.61	63.3	31.3	8.7	31.3	-129.4	
YNG51AB	5.55	765.65	45.8	22.5	11.9	42.5	-112.2	
YNG50AB	5.45	765.70	56.4	34	6.9	37.8	-127.2	
YNG49AB	5.35	765.74	49.6	33.5	9.4	43.2	-122.5	
YNG48AB	5.25	765.78	29.6	60	11.2	66.1	-153.1	
YNG47AB	5.15	765.82	32.2	33.9	9.4	57.1	-108.5	
YNG46AB	5.05	765.87	60.4	33.5	13	34.4	-129.2	
YNG45AB	4.95	765.91	52.3	16.9	4.4	35.5	-114.0	
YNG44AB	4.85	765.95	41.2	34.7	11.5	50.4	-117.3	
YNG43AB	4.75	765.99	30.6	17.3	8.7	51.7	-94.3	
YNG42AB	4.65	766.03	38.2	25	8.7	49.2	-107.2	
YNG41AB	4.55	766.08	39	36.8	7.8	52.9	-117.5	
YNG40AB	4.45	766.12	10.7	34	12.6	71.1	-72.9	
YNG39AB	4.35	766.16	-5.8	53.7	10.7	85.2	42.6	
YNG38AB	4.25	766.20	12.5	49.9	14.5	78.7	-111.2	
YNG37AB	4.15	766.25	-5.7	41.4	16.5	77.7	-14.7	
YNG36AB	4.05	766.29	24.6	45.7	12.2	67.6	-116.3	
YNG35AB	3.95	766.33	20.3	40.6	11.3	68.8	-101.7	
YNG34AB	3.85	766.37	28.7	35.2	11.5	60.3	-106.0	
YNG33AB	3.75	766.41	34.8	53	16.8	61.4	-137.2	
YNG32AB	3.65	766.72	-11.8	-5.6	24.6	50.6	-21.2	
YNG31AB	3.55	767.03	-39.3	39.3	18.4	53.5	40.3	
YNG30AB	3.45	767.34	9.3	44.1	16.1	77.8	-83.7	
YNG29AB	3.35	767.65	-0.8	46.9	22.4	83.1	-34.1	
YNG28AB	3.25	767.97	50.8	50.7	27.1	47.8	-140.1	
YNG27AB	3.15	768.28	2.6	82.8	29.4	49.2	141.0	
YNG26AB	3.05	768.59	-172.7	54.3	43	-19.8	133.6	
YNG25AB	2.95	768.90	-21.9	61.8	20.3	71.3	81.8	
YNG24AB	2.85	769.22	31.2	77	25.6	54.5	162.0	
YNG23AB	2.75	769.53	130.9	70.9	23.1	9.6	165.9	
YNG22AB	2.65	769.84	44	80.2	28	47.3	159.5	
YNG21AB	2.55	770.15	39.3	74.4	16.7	54.1	171.8	
YNG20AB	2.45	770.47	52.4	42	31.4	43.7	-131.4	
YNG19AB	2.35	770.78	130.8	72.5	30.8	11.5	164.3	
YNG18AB	2.25	771.09	15	57.5	30.4	77.6	-149.0	
YNG17AB	2.15	771.40	-28	36.6	37	61.4	26.7	
YNG16AB	2.05	771.72	3.3	39.1	19.7	76.8	-53.5	
YNG15AB	1.95	772.03	20.1	30.3	18.8	64.1	-88.9	
YNG14AB	1.85	772.34	36.7	46.5	20.4	58.0	-127.3	
YNG13AB	1.75	772.65	3.9	66.5	22.6	75.7	150.4	
YNG12AB	1.65	772.97	-15.6	68.2	37.7	70.2	110.3	
YNG11AB	1.55	773.28	20.1	35.1	18.6	66.3	-93.9	
YNG10AB	1.45	773.59	-21.5	34.7	34	65.2	15.7	
YNG09AB	1.35	773.90	76.6	35.4	29.6	21.8	-139.2	
YNG08AB	1.25	774.22	16	45.9	14.4	74.3	-105.0	
YNG07AB	1.15	774.53	147.7	77.7	29.9	14.4	152.7	Transition interval
YNG06AB	1.05	774.84	-94.9	49.3	29.9	13.2	77.8	
YNG05AB	0.95	775.15	88.7	42.5	41.6	14.8	-149.9	
YNG04AB	0.85	775.47	-90.2	14.3	49	4.0	56.1	
Matuyama-Brunhes Boundary								
YNG03AB	0.75	775.78	-120.5	-59	14.6	-43.4	25.6	Transition interval
YNG02AB	0.65	776.09	-114.1	-40.6	26.9	-32.2	42.7	
YNG01AB	0.55	776.40	-115.6	-25.3	14.5	-28.4	53.4	
TBH001AB	0.45	776.71	134.9	-3.9	13.6	-36.7	-158.0	
TBH002AB	0.35	777.03	141.9	-37.2	10.1	-53.7	-142.8	
TBH003AB	0.25	777.34	169.3	-26.9	28.2	-67.1	167.6	
TBH004AB	0.15	777.65	141.4	-29.5	9.8	-50.5	-149.1	
TBH005AB	0.05	777.96	157.5	-27.1	10.5	-61.1	-169.9	
TBH006AB	-0.05	778.28	130.5	-23.7	20.2	-40.0	-144.2	
TBH007AB	-0.15	778.59	131.8	-4.2	25.6	-34.5	-155.3	
TBH008AB	-0.25	778.90	140.1	-16.1	28.4	-44.7	-156.6	
TBH009AB	-0.35	779.21	167.3	-71.7	25.3	-66.8	-57.9	
TBH010AB	-0.45	779.53	172.3	-61.3	16.8	-80.5	-76.7	
TBH011AB	-0.55	779.84	-166	-66.9	10.2	-72.2	-9.1	
TBH012AB	-0.65	780.15	156.2	-61	19.3	-70.2	-102.1	
TBH013AB	-0.75	780.46	135.7	-37.8	19.9	-48.9	-137.6	

TBH014AB	-0.85	780.78	129.7	-54.2	23.2	-49.2	-115.3	
TBH015AB	-0.95	781.09	99	-50	22.4	-23.8	-108.0	
TBH016AB	-1.05	781.40	135.1	-61	17.8	-54.6	-104.8	
TBH017AB	-1.15	781.71	-133.8	-54.5	20.7	-52.5	36.2	
TBH018AB	-1.25	782.03	-154.9	-51.6	23.8	-69.0	50.4	
TBH019AB	-1.35	782.34	-173.6	-29.8	22.1	-70.1	121.6	
TBH020AB	-1.45	782.65	-176.4	-25.4	5.9	-68.1	130.6	
TBH021AB	-1.55	782.96	167.1	-41.8	8	-74.4	-170.8	
TBH022AB	-1.65	783.28	174.3	-40.4	6.3	-77.1	164.1	
TBH023AB	-1.75	783.59	162.7	-41.5	4.8	-71.3	-161.9	
TBH024AB	-1.85	783.90	178.8	-35.5	8.4	-74.6	144.3	
TBH025AB	-1.95	784.21	171.2	-43.1	6.4	-77.5	179.8	
TBH026AB	-2.05	784.53	151.8	-35.4	5.9	-60.7	-154.4	
TBH027AB	-2.15	784.84	171	-40.3	3.7	-75.6	175.5	
TBH028AB	-2.25	785.15	167.4	-52.4	5.3	-79.4	-137.3	
TBH029AB	-2.35	785.46	167	-50.3	3.7	-78.4	-146.2	
TBH030AB	-2.45	785.78	162.4	-49.9	4.2	-74.6	-141.3	
TBH031AB	-2.55	785.97	175.8	-49	2.6	-83.8	176.0	
TBH032AB	-2.65	786.02	168.7	-43.1	7.6	-76.1	-172.4	
TBH033AB	-2.75	786.08	176	-55.1	5.5	-86.7	-117.9	
TBH034AB	-2.85	786.13	179	-57.4	7.8	-86.9	-54.6	
TBH035AB	-2.95	786.18	-169.8	-58.9	4.1	-80.7	17.1	
TBH036AB	-3.05	786.24	161	-59.5	5.3	-74.1	-104.8	
TBH037AB	-3.15	786.29	94	-63.8	4.8	-26.7	-91.5	
TBH038AB	-3.25	786.35	105.7	-67.3	5.7	-35.6	-89.4	
TBH039AB	-3.35	786.40	159.4	-64.6	6.1	-70.7	-87.2	
TBH040AB	-3.45	786.45	138.9	-64.3	4.7	-57.3	-97.5	
TBH041AB	-3.55	786.51	129.4	-72.3	5.7	-49.7	-80.0	
TBH042AB	-3.65	786.56	177	-67.3	6	-74.8	-47.3	
TBH043AB	-3.75	786.62	171.9	-80.2	5.7	-53.8	-44.5	
TBH044AB	-3.85	786.67	175.6	-64.4	5.1	-78.3	-55.2	
TBH045AB	-3.95	786.72	156.1	-65.9	6.5	-67.9	-86.0	
TBH046AB	-4.05	786.78	157.5	-57.9	4.7	-71.7	-112.2	
TBH047AB	-4.15	786.83	163.2	-59.3	5.9	-75.8	-104.0	
TBH048AB	-4.25	786.89	144.1	-66.7	4.4	-60.2	-90.3	
TBH049AB	-4.35	786.94	152.4	-68.4	6.5	-64.2	-81.4	
TBH050AB	-4.45	786.99	166.5	-59.4	13.1	-78.1	-100.0	
TBH051AB	-4.55	787.05	154.4	-41.3	11.6	-65.1	-150.0	
TBH052AB	-4.65	787.10	150.7	-53.4	7.2	-65.9	-124.0	
TBH053AB	-4.75	787.16	144.4	-67.2	8.3	-60.2	-88.9	
TBH054AB	-4.85	787.21	170.3	-53.5	12.1	-82.0	-134.0	
TBH055AB	-4.95	787.26	157.2	-58.9	8.7	-71.3	-108.8	
TBH056AB	-5.05	787.32	145.8	-67.1	8.7	-61.1	-88.6	
TBH057AB	-5.15	787.37	147.9	-59.8	18.2	-64.2	-107.7	
TBH058AB	-5.25	787.43	158.4	-49.8	2.4	-71.4	-137.5	
TBH059AB	-5.35	787.48	151.5	-51	5	-66.0	-129.8	
TBH060AB	-5.45	787.53	155	-66.2	4.1	-67.1	-86.0	
TBH061AB	-5.55	787.59	162.2	-63.8	3.7	-72.9	-86.9	
TBH062AB	-5.65	787.64	144.8	-62.1	4.9	-61.7	-102.1	
TBH063AB	-5.75	787.70	141.8	-70.8	6.3	-57.0	-80.4	
TBH064AB	-5.85	787.75	163.9	-60	5.2	-76.0	-100.3	
TBH065AB	-5.95	787.80	177.7	-56.6	3.6	-87.1	-79.9	
TBH066AB	-6.05	787.86	163.1	-54.3	3.5	-76.2	-125.8	
TBH067AB	-6.15	787.91	171.3	-52.4	6.3	-82.5	-143.1	
TBH068AB	-6.25	787.97	171.1	-50.2	3.4	-81.5	-155.9	
TBH069AB	-6.35	788.02	158	-55.7	6.6	-72.1	-119.6	
TBH070AB	-6.45	788.07	83.8	-47.1	17.6	-11.2	-103.2	
TBH071AB	-6.55	788.13	164	-50.8	7.2	-76.2	-140.1	

Sampling locality			
Sample code	Section name	Latitude	Longitude
TBH	Tabuchi	35˚17.66'N	140˚8.79'E
YNG	Yanagawa	35˚17.15'N	140˚11.89'E

Suganuma et al., S. Table 1

S. Table 2

Sample	Latitude (˚)	Longitude (˚)	Stratigraphic distance from the Byk-E bed (m)	Stratigraphic distance without sand (m)	$\delta^{18}O$ benthic (‰)	Age (ka) based on U1308 chronology[5]	Sedimentation rate (cm/kyr)	Comments
KG02	35.3119	140.1961	52.39	50.32	3.03			
KG03	35.3119	140.1961	51.35	49.28	3.39	745.4	259	tie point
KG04	35.3118	140.1963	49.95	48.49	3.02	745.7	259	
KG05	35.3117	140.1964	47.76	47.76	3.21	746.0	259	
KG07	35.3115	140.1966	45.02	45.02	2.97	747.1	259	
KG08	35.3116	140.1965	44.05	44.05	3.04	747.5	259	
KG09	35.3115	140.1966	42.89	42.89	2.87	747.9	259	
KG10	35.3115	140.1966	41.74	41.74	3.01	748.4	259	
KG11	35.3114	140.1967	40.40	40.40	2.98	748.9	259	
KG12	35.3113	140.1967	39.30	39.30	2.78	749.3	259	
KG13	35.3113	140.1968	38.45	38.45	2.81	749.6	259	
KG14	35.3112	140.1969	37.23	37.23	2.92	750.1	259	
KG15	35.3111	140.1969	36.26	36.26	2.92	750.5	259	
KG16	35.3110	35.3110	34.62	34.62	2.80	751.1	259	
KG17	35.3111	140.1971	33.10	33.10	2.71	751.7	259	
KG18	35.3107	140.1973	32.06	32.06	2.62	752.1	259	
Ku2 tephra			32.00	32.00		752.1	259	
KG19	35.3107	140.1973	30.90	30.90	3.23	752.5	329	tie point
KG20	35.3107	140.1973	29.81	29.81	3.13	752.9	329	
KG21	35.3107	140.1973	28.59	28.59	2.45	753.2	329	
KG22	35.3107	140.1973	27.44	27.44	2.55	753.6	329	
KG23	35.3107	140.1973	26.28	26.28	2.81	753.9	329	
KG24	35.3105	140.1973	25.06	25.06	2.95	754.3	329	
KG25	35.3104	140.1973	23.85	23.85	2.84	754.7	329	
KG26	35.3102	140.1973	22.87	22.87	3.18	755.0	329	
KG27	35.3101	140.1974	21.90	21.90	3.30	755.3	106	tie point
KG28	35.3101	140.1975	20.74	20.74	2.65	756.4	106	
KG29	35.3101	140.1976	19.46	19.46	2.89	757.6	106	
KG30	35.3100	140.1977	18.31	18.31	2.70	758.7	106	
KG31	35.3099	140.1977	17.03	17.03	2.64	759.9	106	
KG32	35.3099	140.1978	15.26	15.26	2.98	761.5	237	tie point, MIS18/19
KG33	35.3098	140.1979	14.11	14.11	2.27	762.0	237	
KG34	35.3097	140.1979	12.89	12.89	2.66	762.6	237	
KG35	35.3096	140.1979	11.67	11.67	2.34	763.1	237	
KG36	35.3094	140.1984	10.40	10.40	2.35	763.6	237	
KG37	35.3093	140.1983	9.12	9.12	2.31	764.1	237	
KG38	35.3092	140.1983	7.60	7.60	2.29	764.8	237	
YG05	35.2856	140.1310	3.75	3.75	2.60	766.4	32	tie point
YG04	35.2856	140.1310	2.73	2.73	2.43	769.6	32	
YG03	35.2856	140.1310	2.20	2.20	2.62	771.3	32	
YG02	35.2856	140.1310	1.34	1.34	2.31	773.9	32	
YG01	35.2856	140.1310	0.73	0.73	2.37	775.8	32	
Byk-E			0.00	0.00		778.1	32	
YN01	35.2856	140.1310	-0.10	-0.10	2.38	778.4	32	
YN02	35.2856	140.1310	-0.92	-0.92	2.42	781.0	32	
YN03	35.2856	140.1310	-2.03	-2.03	2.22	784.5	32	
YN20	35.2856	140.1310	-2.71	-2.71	2.20	786.1	185	tie point
YN18	35.2856	140.1310	-4.60	-4.60	2.43	787.1	185	
YN17	35.2856	140.1310	-5.81	-5.81	2.54	787.7	185	
YN16	35.2855	140.1303	-6.82	-6.73	2.69	788.2	185	
YN15	35.2855	140.1303	-7.50	-7.31	2.96	788.7	118	tie point
YN14	35.2855	140.1303	-8.47	-8.08	2.98	789.4	118	
YN13	35.2855	140.1303	-9.19	-8.71	3.05	789.9	118	
YN12	35.2855	140.1303	-10.16	-9.58	3.04	790.6	118	MIS 19/20
YN11	35.2855	140.1303	-11.14	-9.65	3.09	790.7	118	
YN10	35.2851	140.1306	-11.70	-10.21	3.05	791.2	118	
YN07	35.2851	140.1306	-13.37	-11.16	3.03	792.0	118	
YN09	35.2851	140.1306	-14.25	-12.04	3.15	792.7	118	
YN06	35.2851	140.1306	-15.36	-12.43	3.33	793.1	118	
YN05	35.2850	140.1307	-16.56	-13.45	3.05	793.9	118	
YN04	35.2850	140.1307	-18.07	-14.78	3.17	795.1	118	
YN08	35.2850	140.1307	-20.54	-15.45	3.15	795.6	118	
YW01	35.2813	140.1245	-28.20	-17.69	3.31	797.5	118	
YW02	35.2813	140.1245	-29.58	-18.72	3.47	798.4	391	tie point
YW03	35.2813	140.1245	-31.40	-20.36	3.28	798.8	391	
YW06	35.2813	140.1245	-35.98	-23.04	3.29	799.5	391	
YW07	35.2813	140.1245	-37.62	-24.51	3.36	799.9	391	
YW09	35.2804	140.1245	-45.81	-26.37	3.29	800.4	391	
YW10	35.2804	140.1245	-47.16	-27.48	2.95	800.7		tie point
YW11	35.2804	140.1245	-47.80	-27.88	3.14			

S. Table 3A

Spot	Pb_c %	U ppm	Th ppm	^{204}Pb correction ppm	Th/U	disequilibrium uncorrected: ^{204}Pb correction age (Ma) ^{206}Pb/^{238}U	^{204}Pb correction age (Ma) ^{207}Pb/^{206}Pb	^{238}U/^{206}Pb*	±%	^{206}Pb* / ^{207}Pb*	±%	^{207}Pb*/^{235}U	±%	^{206}Pb*/^{238}U	±%	err corr	^{207}Pb correction age (Ma) ^{206}Pb/^{238}U	^{207}Pb correction ^{206}Pb*/^{238}U	±%	^{230}U-^{238}Th disequilibrium corrected: ^{204}Pb correction age (Ma) ^{206}Pb/^{238}U	^{204}Pb correction ^{206}Pb*/^{238}U	±%	^{207}Pb correction age (Ma) ^{206}Pb/^{238}U	^{207}Pb correction ^{206}Pb*/^{238}U	±%
TNTT3-3.1	16.33	78	68	0.0069	0.90	0.68 ±0.12	773 ±4248	9479	16.9	0.0649	202	0.00094	203	0.000106	16.9	0.1	0.66 ±0.03	0.000103	1.4	0.77 ±0.12	0.000120	15.0	0.76 ±0.01	0.000117	1.6
TNTT3-7.1	22.73	64	48	0.0055	0.78	0.65 ±0.19	171 ±10934	9969	29.8	0.0495	468	0.00068	469	0.000100	29.8	0.1	0.64 ±0.06	0.000100	3.0	0.74 ±0.19	0.000115	26.1	0.74 ±0.02	0.000114	2.8
TNTT3-14.1	0.65	45	35	0.0040	0.81	0.68 ±0.14	249 ±658	9452	20.2	0.0512	29	0.00075	35	0.000106	20.2	0.6	0.68 ±0.14	0.000105	6.5	0.78 ±0.14	0.000120	17.8	0.77 ±0.04	0.000120	5.8
TNTT3-16.1	20.67	135	134	0.0124	1.03	0.71 ±0.11	911 ±3740	9050	16.1	0.0694	182	0.00106	182	0.000110	16.1	0.1	0.69 ±0.04	0.000107	1.7	0.80 ±0.11	0.000124	14.3	0.78 ±0.01	0.000121	1.8
TNTT3-17.1	0.26	45	47	0.0039	1.10	0.67 ±0.09	105 ±621	9672	13.8	0.0481	26	0.00069	30	0.000103	13.8	0.5	0.66 ±0.09	0.000103	4.4	0.75 ±0.09	0.000117	12.3	0.75 ±0.03	0.000117	4.1
TNTT3-18.2	0.66	36	35	0.0032	1.02	0.68 ±0.04	254 ±750	9447	5.2	0.0513	33	0.00075	33	0.000106	5.2	0.2	0.68 ±0.04	0.000105	1.8	0.77 ±0.04	0.000120	4.7	0.77 ±0.01	0.000119	1.9
TNTT3-20.1	41.18	47	40	0.0043	0.86	0.68 ±0.34	142 ±18875	9504	49.7	0.0489	804	0.00071	806	0.000105	49.7	0.1	0.68 ±0.08	0.000105	3.6	0.77 ±0.34	0.000120	43.8	0.77 ±0.03	0.000119	3.3
TNTT2-2.1	0.13	205	437	0.0183	2.20	0.67 ±0.04	53.5 ±654	9635	5.5	0.0471	27	0.00067	28	0.000104	5.5	0.2	0.67 ±0.04	0.000104	1.8	0.74 ±0.04	0.000114	5.1	0.74 ±0.01	0.000114	2.0
TNTT2-24.1	29.17	46	43	0.0041	0.97	0.68 ±0.28	215 ±14808	9545	40.9	0.0504	639	0.00073	641	0.000105	40.9	0.1	0.67 ±0.06	0.000104	2.9	0.77 ±0.28	0.000119	36.1	0.76 ±0.02	0.000118	2.8
TNTT2-7.1	0.59	100	151	0.0094	1.55	0.70 ±0.05	230 ±450	9161	6.6	0.0508	19	0.00076	21	0.000109	6.6	0.3	0.70 ±0.05	0.000109	2.1	0.78 ±0.05	0.000122	6.1	0.78 ±0.02	0.000121	2.5
TNTT2-25.1	41.58	36	40	0.0032	1.15	0.69 ±0.48	482 ±21245	9374	69.8	0.0567	962	0.00083	964	0.000107	69.8	0.1	0.68 ±0.10	0.000105	4.9	0.77 ±0.48	0.000120	61.9	0.77 ±0.03	0.000119	4.5
TNTT2-26.1	28.03	73	72	0.0066	1.02	0.69 ±0.27	117 ±15037	9397	38.7	0.0484	638	0.00071	639	0.000106	38.7	0.1	0.68 ±0.05	0.000106	2.3	0.78 ±0.27	0.000120	34.2	0.77 ±0.02	0.000120	2.2
TNTT2-26.2	1.08	113	109	0.0104	1.00	0.70 ±0.05	395 ±494	9224	7.4	0.0546	22	0.00082	23	0.000108	7.4	0.3	0.69 ±0.05	0.000107	2.4	0.79 ±0.05	0.000122	6.6	0.78 ±0.02	0.000121	2.3
TNTT2-27.1	16.07	110	163	0.0098	1.52	0.67 ±0.13	-6 ±8089	9637	20.0	0.0459	335	0.00066	336	0.000104	20.0	0.1	0.67 ±0.04	0.000104	2.1	0.75 ±0.13	0.000116	17.9	0.75 ±0.02	0.000116	2.1
TNTT2-32.1	0.19	41	40	0.0038	1.00	0.70 ±0.07	75.7 ±865	9207	9.4	0.0475	36	0.00071	38	0.000109	9.4	0.2	0.70 ±0.07	0.000108	3.1	0.79 ±0.07	0.000123	8.4	0.79 ±0.02	0.000122	3.1
TNTT2-16.1	1.09	60	59	0.0053	1.02	0.67 ±0.08	398 ±619	9651	12.0	0.0547	28	0.00078	30	0.000104	12.0	0.4	0.66 ±0.08	0.000102	3.9	0.76 ±0.08	0.000118	10.7	0.75 ±0.03	0.000116	3.6
TNTT2-38.1	1.07	76	82	0.0069	1.12	0.69 ±0.03	392 ±506	9293	4.4	0.0545	23	0.00081	23	0.000108	4.4	0.2	0.69 ±0.03	0.000106	1.5	0.78 ±0.03	0.000121	4.0	0.77 ±0.01	0.000120	1.6
TNTT2-40.1	--	108	177	0.0100	1.70	0.69 ±0.03	-95 ±532	9294	3.8	0.0443	22	0.00066	22	0.000108	3.8	0.2	0.70 ±0.03	0.000108	1.3	0.77 ±0.03	0.000120	3.6	0.77 ±0.01	0.000120	1.6
TNTT4-1.1	0.13	157	211	0.0146	1.39	0.70 ±0.009	54.8 ±110	9212	1.3	0.0471	5	0.00071	5	0.000109	1.3	0.3	0.70 ±0.009	0.000108	0.4	0.78 ±0.05	0.000121	5.8	0.78 ±0.01	0.000121	1.7
TNTT4-5.1	0.03	71	31	0.0064	0.45	0.68 ±0.008	15.1 ±143	9482	1.2	0.0463	6	0.00067	6	0.000105	1.2	0.2	0.68 ±0.009	0.000105	0.4	0.78 ±0.13	0.000121	16.6	0.78 ±0.02	0.000121	2.6
TNTT4-8.1	14.91	132	110	0.0120	0.86	0.68 ±0.05	52.1 ±3459	9421	6.7	0.0471	145	0.00069	145	0.000106	6.7	0.0	0.68 ±0.04	0.000106	1.8	0.78 ±0.09	0.000121	11.0	0.78 ±0.05	0.000121	6.2
TNTT4-9.1	0.32	212	142	0.0194	0.69	0.69 ±0.008	86.4 ±674	9355	1.2	0.0477	28	0.00070	28	0.000107	1.2	0.0	0.69 ±0.01	0.000107	0.7	0.78 ±0.07	0.000122	9.6	0.78 ±0.02	0.000122	2.1
TNTT4-9.2	1.22	216	158	0.0191	0.76	0.66 ±0.01	25.5 ±448	9715	2.1	0.0465	19	0.00066	19	0.000103	2.1	0.1	0.66 ±0.01	0.000103	0.7	0.76 ±0.07	0.000118	9.1	0.76 ±0.02	0.000118	2.6
TNTT4-31.1	0.24	62	62	0.0058	1.03	0.70 ±0.01	52.6 ±259	9222	1.9	0.0471	11	0.00070	11	0.000108	1.9	0.2	0.70 ±0.01	0.000108	0.6	0.79 ±0.07	0.000122	8.6	0.79 ±0.02	0.000122	2.2

S. Table 3B

Spot	Pb_c %	U ppm	Th ppm	^{204}Pb correction ppm	Th/U	disequilibrium uncorrected: ^{204}Pb correction age (Ma) ^{206}Pb/^{238}U	^{204}Pb correction age (Ma) ^{207}Pb/^{206}Pb	^{238}U/^{206}Pb*	±%	^{206}Pb* / ^{207}Pb*	±%	^{207}Pb*/^{235}U	±%	^{206}Pb*/^{238}U	±%	err corr	^{207}Pb correction age (Ma) ^{206}Pb/^{238}U	^{207}Pb correction ^{206}Pb*/^{238}U	±%	^{230}U-^{238}Th disequilibrium corrected: ^{204}Pb correction age (Ma) ^{206}Pb/^{238}U	^{204}Pb correction ^{206}Pb*/^{238}U	±%	^{207}Pb correction age (Ma) ^{206}Pb/^{238}U	^{207}Pb correction ^{206}Pb*/^{238}U	±%
TNTT-1.1	0.15	425	406	3.7	0.99	65.65 ±0.55	94.1 ±52	98	0.8	0.0479	2	0.06760	2	0.010236	0.8	0.4	65.60 ±0.55	0.010229	0.3						
TNTT-3.1	--	276	128	0.4	0.48	11.40 ±0.23	36.3 ±100	565	2.0	0.0467	4	0.01141	5	0.001771	2.0	0.4	11.40 ±0.23	0.001770	0.7						
TNTT-4.1	0.23	131	91	1.2	0.72	66.52 ±0.54	67.7 ±142	96	0.8	0.0474	6	0.06774	6	0.010373	0.8	0.1	66.52 ±0.55	0.010372	0.3						
TNTT-5.1	0.07	393	184	3.5	0.48	67.05 ±0.50	103 ±45	96	0.8	0.0481	2	0.06931	2	0.010456	0.8	0.4	66.99 ±0.50	0.010446	0.2						
TNTT-6.1	1.68	3026	376	27.4	0.13	67.69 ±0.38	224 ±103	95	0.6	0.0506	4	0.07368	4	0.010556	0.6	0.1	67.42 ±0.40	0.010513	0.2						
TNTT-7.1	0.68	616	260	5.4	0.44	65.94 ±0.51	20.0 ±84	97	0.8	0.0464	3	0.06582	4	0.010281	0.8	0.2	66.01 ±0.50	0.010293	0.2						
TNTT-9.1	0.32	522	529	4.6	1.05	65.42 ±0.41	23.2 ±66	98	0.6	0.0465	3	0.06539	3	0.010200	0.6	0.2	65.49 ±0.40	0.010211	0.2						
TNTT-11.1	0.02	2957	1392	27.2	0.49	68.54 ±0.37	85.8 ±13	94	0.5	0.0477	1	0.07035	1	0.010690	0.5	0.7	68.52 ±0.37	0.010685	0.2						
TNTT-12.1	0.06	284	145	8.5	0.53	222 ±1.84	281 ±25	29	0.8	0.0519	1	0.25037	1	0.034988	0.8	0.6	221 ±1.85	0.034930	0.3						
TNTT-13.1	--	102	73	0.0	0.74	0.80 ±0.06	255 ±550	8031	7.1	0.0513	24	0.00088	25	0.000125	7.1	0.3	0.80 ±0.06	0.000124	2.3						
TNTT-14.1	--	532	183	27.2	0.36	373 ±2.61	378 ±16	17	0.7	0.0542	1	0.44518	1	0.059610	0.7	0.7	373 ±2.65	0.059601	0.2						
TNTT-15.1	0.00	502	276	4.6	0.57	68.47 ±0.41	83.3 ±29	94	0.6	0.0477	1	0.07020	1	0.010678	0.6	0.4	68.45 ±0.42	0.010674	0.2						
TNTT-16.1	0.07	173	57	49.1	0.34	1842 ±11.69	1881 ±6	3	0.7	0.1151	0	5.24764	1	0.330760	0.7	0.9	1837 ±13.17	0.329713	0.3						
TNTT-17.1	0.39	2092	854	18.5	0.42	66.17 ±0.41	53.5 ±35	97	0.6	0.0471	1	0.06698	2	0.010318	0.6	0.4	66.19 ±0.41	0.010321	0.2						
TNTT-18.1	0.33	1503	569	14.6	0.39	72.24 ±0.41	84.2 ±33	89	0.6	0.0477	1	0.07411	1	0.011269	0.6	0.4	72.22 ±0.41	0.011266	0.2						
TNTT-20.1	0.00	307	147	2.8	0.49	67.04 ±0.52	82.7 ±37	96	0.8	0.0477	2	0.06871	2	0.010454	0.8	0.4	67.02 ±0.53	0.010450	0.3						
TNTT-21.1	0.02	217	47	59.5	0.22	1788 ±10.79	1887 ±4	3	0.7	0.1155	0	5.08835	1	0.319618	0.7	0.9	1776 ±12.00	0.317090	0.2						
TNTT-22.1	0.00	125	97	1.1	0.80	64.81 ±0.71	77.9 ±60	99	1.1	0.0476	3	0.06628	3	0.010105	1.1	0.4	64.79 ±0.72	0.010102	0.4						
TNTT-23.1	0.18	178	83	1.6	0.48	66.87 ±0.92	60.1 ±91	96	1.4	0.0472	4	0.06788	4	0.010427	1.4	0.3	66.88 ±0.92	0.010429	0.4						
TNTT-24.1	0.00	240	208	2.1	0.90	66.77 ±0.45	96.5 ±41	96	0.7	0.0479	2	0.06883	2	0.010412	0.7	0.4	66.72 ±0.45	0.010404	0.2						
TNTT-25.1	0.20	295	195	2.6	0.68	66.56 ±0.44	3.7 ±71	96	0.7	0.0461	3	0.06600	3	0.010379	0.7	0.2	66.67 ±0.44	0.010395	0.2						
TNTT-26.1	0.37	72	27	0.6	0.39	63.41 ±2.58	97.0 ±165	101	4.1	0.0480	7	0.06536	8	0.009884	4.1	0.5	63.35 ±2.57	0.009876	1.3						
TNTT-27.1	0.60	48	42	0.4	0.89	63.13 ±1.11	48.3 ±265	102	1.8	0.0470	11	0.06375	11	0.009841	1.8	0.2	63.15 ±1.05	0.009845	0.5						
TNTT-28.1	--	177	101	1.6	0.59	67.23 ±0.81	140 ±81	95	1.2	0.0488	3	0.07059	4	0.010484	1.2	0.3	67.11 ±0.83	0.010465	0.4						
TNTT-31.1	--	36	44	0.0	1.27	2.60 ±0.15	27.3 ±557	2478	5.9	0.0466	23	0.00259	24	0.000403	5.9	0.2	2.60 ±0.16	0.000403	1.9						
TNTT-32.1	0.00	838	203	326.2	0.25	2410 ±14.27	2436 ±10	2	0.7	0.1582	1	9.88318	1	0.453226	0.7	0.8	2403 ±18.13	0.451657	0.3						
TNTT-33.1	0.04	352	43	99.3	0.13	1829 ±10.13	1880 ±4	3	0.6	0.1150	0	5.20251	1	0.328089	0.6	1.0	1823 ±11.37	0.326739	0.2						
TNTT-37.1	0.46	137	56	1.2	0.42	65.50 ±0.55	51.3 ±159	98	0.8	0.0470	7	0.06624	7	0.010212	0.8	0.1	65.52 ±0.53	0.010216	0.3						
TNTT-38.1	0.07	162	62	46.6	0.39	1859 ±12.11	1876 ±8	3	0.8	0.1148	0	5.28991	1	0.334293	0.8	0.9	1857 ±13.72	0.333824	0.3						
TNTT-39.1	0.83	76	60	0.7	0.82	65.66 ±0.72	-76 ±272	98	1.1	0.0446	11	0.06300	11	0.010237	1.1	0.1	65.88 ±0.63	0.010272	0.3						
TNTT-40.1	0.01	491	716	143.7	1.51	1891 ±10.04	1880 ±3	3	0.6	0.1150	0	5.40540	1	0.340923	0.6	1.0	1893 ±11.43	0.341245	0.2						
TNTT-41.1	0.14	242	74	2.1	0.32	65.19 ±0.57	99.0 ±71	98	0.9	0.0480	3	0.06726	3	0.010164	0.9	0.3	65.14 ±0.57	0.010156	0.3						
TNTT-43.1	0.39	83	49	0.8	0.62	68.33 ±0.68	26.4 ±180	94	1.0	0.0466	8	0.06840	8	0.010657	1.0	0.1	68.41 ±0.64	0.010668	0.3						
TNTT-44.1	10.37	79	39	0.0	0.51	2.31 ±0.35	219 ±4244	2793	15.1	0.0505	183	0.00249	184	0.000358	15.1	0.1	2.29 ±0.23	0.000356	3.2						
TNTT-45.1	--	301	116	2.7	0.40	67.38 ±0.68	-9 ±41	95	1.0	0.0459	2	0.06647	2	0.010508	1.0	0.5	67.51 ±0.69	0.010527	0.3						
TNTT-46.1	0.16	454	230	16.0	0.52	259 ±1.58	250 ±24	24	0.6	0.0512	1	0.28945	1	0.041003	0.6	0.5	259 ±1.59	0.041013	0.2						
TNTT-47.1	--	985	433	8.9	0.45	67.71 ±0.39	61.9 ±22	95	0.6	0.0472	1	0.06879	1	0.010558	0.6	0.5	67.72 ±0.39	0.010560	0.2						
TNTT-48.1	--	226	133	0.1	0.61	2.53 ±0.09	879 ±189	2547	3.5	0.0684	9	0.00370	10	0.000393	3.5	0.4	2.46 ±0.09	0.000382	1.1						
TNTT-50.1	0.26	665	266	5.9	0.41	66.62 ±0.60	73.8 ±77	96	0.9	0.0475	3	0.06802	3	0.010389	0.9	0.3	66.61 ±0.60	0.010387	0.3						
TNTT-57.1	6.80	120	59	0.0	0.51	2.45 ±0.19	178 ±2745	2627	7.9	0.0496	118	0.00261	118	0.000381	7.9	0.1	2.44 ±0.08	0.000379	1.1						
TNTT4-30.1	1.78	58	48	0.0056	0.85	0.72 ±0.01	57.8 ±311	8912	1.5	0.0472	13	0.00073	13	0.000112	1.5	0.1	0.72 ±0.01	0.000112	0.5						

Errors are 1-sigma; Pb_c and Pb^* indicate the common and radiogenic portions, respectively.

Error in Standard calibration was 0.24% (not included in above errors but required when comparing data from different mounts).

^{204}Pb correction: Common Pb corrected using measured ^{204}Pb.

^{207}Pb correction: Common Pb corrected by assuming ^{206}Pb/^{238}U-^{207}Pb/^{235}U age-concordance

Suganuma et al., S. Table 3